HHS Public Access

Author manuscript

Neuroimage. Author manuscript; available in PMC 2020 October 01.

Published in final edited form as:

Neuroimage. 2019 October 01; 199: 718–729. doi:10.1016/j.neuroimage.2017.05.023.

Foundations of layer-specific fMRI and investigations of neurophysiological activity in the laminarized neocortex and olfactory bulb of animal models

Alexander John Poplawsky[a,*], **Mitsuhiro Fukuda**[a], **Seong-Gi Kim**[b,c]

[a]Neuroimaging Laboratory, Department of Radiology, University of Pittsburgh, Pittsburgh, PA, USA

[b]Center for Neuroscience Imaging Research, Institute of Basic Science, Suwon 440-746, Republic of Korea

[c]Department of Biomedical Engineering, Sungkyunkwan University, Suwon 440-746, Republic of Korea

Abstract

Laminar organization of neuronal circuits is a recurring feature of how the brain processes information. For instance, different layers compartmentalize different cell types, synaptic activities, and have unique intrinsic and extrinsic connections that serve as units for specialized signal processing. Functional MRI is an invaluable tool to investigate laminar processing in the *in vivo* human brain, but it measures neuronal activity indirectly by way of the hemodynamic response. Therefore, the accuracy of high-resolution laminar fMRI depends on how precisely it can measure localized microvascular changes nearest to the site of evoked activity. To determine the specificity of fMRI responses to the true neurophysiological responses across layers, the flexibility to invasive procedures in animal models has been necessary. In this review, we will examine different fMRI contrasts and their appropriate uses for layer-specific fMRI, and how localized laminar processing was examined in the neocortex and olfactory bulb. Through collective efforts, it was determined that microvessels, including capillaries, are regulated within single layers and that several endogenous and contrast-enhanced fMRI contrast mechanisms can separate these neural-specific vascular changes from the nonspecific, especially cerebral blood volume-weighted fMRI with intravenous contrast agent injection. We will also propose some open questions that are relevant for the successful implementation of layer-specific fMRI and its potential future directions to study laminar processing when combined with optogenetics.

Keywords

BOLD; cerebral blood volume; cerebral blood flow; neocortex; olfactory bulb

[*]Correspondence: Alexander John Poplawsky: McGowan Institute for Regenerative Medicine, University of Pittsburgh, 3025 E. Carson St., Pittsburgh, PA 15203. ajp94@pitt.edu.

1. Introduction

Functional magnetic resonance imaging (fMRI) (Ogawa et al., 1990; Ogawa et al., 1992) is a popular tool to examine brain function because it can noninvasively and longitudinally examine neuronal activity of the entire brain, including structures deep below the cortical surface that are often off-limits to other imaging techniques, like optical imaging. In addition, MRI has a wide assortment of applications and contrasts that make it ideal for multimodal comparisons, such as anatomical and metabolic changes, to the functional and resting-state conditions of the normal and diseased brain. As limitations on the fMRI sensitivity and total scan time decrease (e.g., multi-channel arrays, parallel imaging, compressed-sensing, etc.), high spatial resolution imaging with a sufficient signal-to-noise ratio (SNR) becomes increasingly feasible. However, fMRI measures the vascular or hemodynamic responses to the increased metabolic demand of working neurons and is, therefore, an indirect measure of neuronal responses. This creates a biological limitation imposed by vasculatures on the spatial resolution of fMRI; whereby we must challenge whether the signal changes detected by fMRI are specific to the site of neuronal activity at resolutions capable of discerning brain laminae. To gain such insights, the cortical laminar model has been used both in human (e.g., (Huber et al., 2015; Koopmans et al., 2010; Polimeni et al., 2010; Ress et al., 2007)) and animals (e.g., (Chen et al., 2013; Duong et al., 2000b; Goense et al., 2012; Herman et al., 2013; Lu et al., 2004; Silva and Koretsky, 2002; Zhao et al., 2006)). Particularly, animal models are necessary because of their flexibility toward invasive study, especially electrophysiology and long scanning times, to critically evaluate how different forms of fMRI can be used to acquire and accurately report laminar activations.

In the following review, we will examine the development of laminar-resolution fMRI with animal models and the promising applications of this technique for investigating laminar circuit function of the *in vivo* brain. We will first examine how different fMRI techniques are sensitive to different vascular compartments; and which have better specificity to the microvessels localized to the synaptic activity. Although blood oxygenation level-dependent (BOLD) contrast is often a traditional choice due to its endogenous nature and its translatability to humans, its activation patterns are often contaminated by large vascular contributions distal to the site of neuronal activity. Therefore, we will discuss alternative methods that have a greater specificity and are better suited for preclinical applications, especially at high resolutions. We will then review how fMRI has been used to measure neural-specific responses in the laminated neocortex and olfactory bulb. Specifically, we will review how invasive procedures in animal models are used to investigate the spatial specificity of fMRI to neuronally active sites and the neuronal origins of fMRI signal changes. These studies have provided promising evidence that microvessels, including capillaries, are being regulated by the local synaptic activity of excitatory and inhibitory neurons within individual layers. Please consult Attwell et al. (2010) for a more thorough review of the underlying neurovascular coupling mechanisms found at cellular scales and Gagnon et al. (2015) for detailing the transformation of these microvascular signals to the macrovascular fMRI responses. Finally, we will postulate on the future directions of laminar fMRI as it transitions from a focus on technical development to the practical study of circuit-

level neuroscience. This trend toward neuroscience application will likely be fueled by the growing bank of transgenic animal models that are constructed to probe very specific neuronal processes of normal brain function and dysfunction in models of human disease. Functional MRI is particularly important with these models because it has a dynamic field-of-view, allowing us to explore function of the whole brain and targeted laminar resolution studies of discrete neuronal circuits. Preclinical fMRI can further direct invasive neurophysiological study of laminar circuits to better explore the neuronal underpinnings.

2. Different fMRI contrasts and their specificity to the site of laminar activity

Recent neurovascular coupling studies support that small vessels are regulated near the site of synaptic activity (Hall et al., 2014; Mishra et al., 2016) although the exact mechanism still needs to be resolved (Fernández-Klett et al., 2010; Hill et al., 2015; Kisler et al., 2017). However, the vasculature is hierarchically connected so that local responses will have up- and downstream effects on vessels far from the site of neuronal activity. Because the utility of laminar-resolution fMRI is contingent on separating these neural-specific responses from the nonspecific, many different forms of fMRI contrasts have been examined in preclinical models. The foremost fMRI contrast is BOLD, because it is completely endogenous and easy to implement. BOLD contrast is sensitive to the relative concentration changes of paramagnetic deoxyhemoglobin induced by the increased metabolic demand of evoked neurons, such that decreased deoxyhemoglobin reduces magnetic susceptibilities and increases the fMRI signal. The typical BOLD response is composed of cerebral blood flow (CBF) increases that contribute positively to BOLD signals (i.e., decreases the absolute deoxyhemoglobin concentrations), and cerebral blood volume (CBV) and cerebral metabolic rate of oxygen ($CMRO_2$) increases that contribute negatively to BOLD signals (i.e., increases the absolute deoxyhemoglobin concentrations). Other forms of contrast are often more difficult to implement, have a lesser sensitivity to hemodynamic changes, or require an exogenous contrast agent, but are more successful at measuring the neural-specific responses by weighing the fMRI sensitivity toward a single vascular parameter (e.g., CBF or CBV measurements only) and toward microvascular compartments. The strength of the static magnetic field (B_0) also greatly affects the fMRI signal source so, for the purposes of this review, we will primarily discuss the signal sources at higher magnetic fields, since animal studies are typically performed at these fields.

A long-standing benchmark for the neural-specificity of fMRI is manganese-enhanced MRI (MEMRI) because it directly maps electrically active neurons (Lin and Koretsky, 1997) (for review, see Silva (2012)). Manganese ions principally pass through the cell membrane and into functioning neurons through calcium channel openings, such as voltage-gated calcium channels concentrated at synapses, where they become intracellularly sequestered. A regional manganese increase shortens the longitudinal relaxation time (T1) and is detectable with associated MRI techniques. Manganese cannot be used for human study because it is highly neurotoxic and is limited to only a single stimulation condition. However, its ability to directly map neuronal activity has made it an excellent tool to assess the layer-specificity of different fMRI contrasts.

2.1 Blood oxygenation level-dependent (BOLD) fMRI

Endogenous BOLD contrast was the first fMRI technique described by Ogawa et al. (1990) and is still the primary application of fMRI almost 30 years later. However, the physiological origins of BOLD are complex and are dependent on the imaging technique and parameters (for review, see Kim and Ogawa (2012)). In the scope of laminar fMRI, we will compare the most prominent BOLD technique, gradient-echo (GE), with spin-echo (SE) BOLD because of its improved neural-specificity.

Gradient-echo (GE) BOLD is the most common fMRI technique because it is simple to obtain relatively large evoked signal changes without the introduction of a contrast agent. The typical BOLD response has three main phases due to differences in the temporal dynamics and relative amplitudes of CBF, CBV, and $CMRO_2$. The “initial dip” is characterized as a signal decrease that occurs shortly after the stimulus onset and is believed to be dominated by $CMRO_2$ increases (Ernst and Hennig, 1994; Malonek and Grinvald, 1996; Thompson et al., 2003; Vanzetta and Grinvald, 1999). However, it could be caused by the early onset of arteriole CBV increases occurring before the larger blood oxygenation increases (Sirotin et al., 2009). Although the exact source of the initial dip is still debatable, this negative activation is highly specific to the neuronal activity but has a small amplitude and a short duration (Kim et al., 2000), which makes its detection difficult and unreliable with high resolution fMRI due to its limited sensitivity and temporal resolution (Jezzard et al., 1997) (for review, see Hu and Yacoub (2012)); especially compared to more sensitive and faster techniques, like optical intrinsic signal imaging, where measurement of the initial dip is more commonplace (Malonek and Grinvald, 1996). The initial dip is followed by a large “positive response”, dominated by CBF increases, and is the most significant contributor to the BOLD activation maps. However, this component is primarily sensitive to oxygenation increases in venous vessels, including emerging and pial surface veins and, thus, produces activation maps that are significantly contaminated by nonspecific activation. Regions of large total and venous blood volumes, such as the cortical surface where these large pial vessels reside, are strongly activated and have little neurophysiological bases (Fig. 1A). However, high temporal resolution fMRI with GE BOLD contrast has shown that the earliest positive response is highly layer-specific (Silva and Koretsky, 2002; Silva et al., 2000; Yu et al., 2014), likely due to the early response of capillaries and the delayed onset of nonspecific draining veins. Therefore, fast imaging techniques can allow us to map input layers based on the onset time of endogenous GE BOLD responses. It is also noted that extravascular dephasing around large vessels increases linearly with B_0 and increases supralinearly around microvessels; while intravascular contributions become negligible at high magnetic fields as the transverse relaxation times (T2 and T2*) of blood decreases (Lee et al., 1999; Ogawa et al., 1998; Weisskoff et al., 1994). Therefore, the spatial specificity of the positive response will increase with magnetic field strength. The final phase is a smaller amplitude negative signal change defined as the “post-stimulus undershoot” that is likely caused by prolonged CBV and $CMRO_2$ effects compared to CBF (Hua et al., 2011; Jin and Kim, 2008b; Mandeville et al., 1999). Like the initial dip, the post-stimulus undershoot is more specific than the positive response (Chen and Pike, 2009; Poplawsky et al., 2015; Zhao et al., 2007), but its detection is not always consistent, varies with stimulation type and duration, and its neuronal interpretation may not be straightforward (for review, see van Zijl

et al. (2012)). Due to the complicated nature of both the initial dip and post-stimulus undershoot, these components are rarely used in laminar fMRI studies despite evidence that they have greater neural-specificity compared to the positive response; but there is a clear need to better understand them for high resolution applications. In this way, the positive response remains the principle phase for laminar BOLD fMRI.

Spin-echo (SE) BOLD is a better alternative to GE BOLD when endogenous contrast is necessary because it reduces nonspecific signal changes around large blood vessels and is more sensitive to microvascular compartments (Boxerman et al., 1995). During the echo time (TE), water spins are diffusing and experiencing different susceptibility effects depending on the local environment. Venous vessels create relatively large susceptibility gradients across space due to their higher concentration of paramagnetic deoxyhemoglobin; however, these effects are closely related to the venous vessel size and geometry. If the vessel is large, the susceptibility differences that the spins experience are small and the 180° radiofrequency pulse can refocus them well, reducing the susceptibility effect. However, if the vessel is small, the susceptibility differences are large and the 180° radiofrequency pulse cannot refocus the spins well, preserving the dephasing effects. Therefore, SE BOLD is sensitive to extravascular spins around microvessels at high magnetic fields. Lee et al. (1999) showed that the major source of BOLD changes at 9.4 T are indeed from extravascular water dephasing and that the neural-specificity of SE is increased relative to GE. This is specifically observed as the site of the greatest BOLD activations shift from the brain surface to the parenchyma with GE and SE fMRI, respectively (Fig. 1A–B) (Goense and Logothetis, 2006; Markuerkiaga et al., 2016; Zhao et al., 2004). However, SE fMRI has a poorer sensitivity and temporal resolution compared to GE, so exploration of additional contrasts for preclinical application was necessary.

2.2 Cerebral blood flow (CBF) and cerebral blood volume (CBV) fMRI

One fundamental flaw of BOLD contrast for laminar resolution fMRI is the complexity of its signal source leading to the opposing interactions of CBF and CBV/$CMRO_2$. For example, if the positive and negative effects of these parameters were balanced nearest to the site of neuronal activity, then the neural-specific BOLD signal changes would be negated (Duong et al., 2000a; Moon et al., 2007). To bypass this issue, measurement of a single hemodynamic parameter should provide a clearer interpretation of the neural-specific fMRI changes, especially if hemodynamic changes are concentrated in these sites.

First, CBF fMRI was shown to have improved neural-specificity compared to GE BOLD and to overlap well with layers that have increased calcium-dependent synaptic activity determined by MEMRI (Fig. 1C–E) (Duong et al., 2001; Duong et al., 2000b). However, although being noninvasive, CBF fMRI is more difficult to implement and has a lower sensitivity compared to GE BOLD fMRI. CBF contrast is typically achieved by arterial spin-labeling, where intravascular blood spins are labeled outside of the imaging volume (e.g., the neck) before flowing into the region-of-interest (ROI) (Detre et al., 1992; Kim, 1995; Kwong et al., 1995; Silva and Kim, 1999). This technique is not straightforward to implement because it is best performed using two specialized and actively decoupled surface coils and the transit time for the spins to travel from the neck to the specific ROI must be

considered to optimize the fMRI sensitivity. In addition, the choice of spin-labeling time will greatly affect which vascular compartment the signal changes preferentially originate from and, subsequently, its neural-specificity. For instance, Zappe et al. (2008) observed the greatest signal change at the brain surface and middle layers of the cortex with a short and long spin-labeling time, respectively, which is likely due to the selective targeting of pial arteries and microvessels, respectively.

Second, contrast-enhanced CBV-weighted (CBVw) fMRI is advantageous for preclinical models because it can easily be achieved with intravenous injection of superparamagnetic iron oxide nanoparticles (e.g., MION) (Mandeville et al., 2004; Mandeville et al., 1998). Such agents have long half-lives and dose-dependently eliminate the signal from the blood by increasing intravascular magnetic susceptibilities and severely reducing blood T2*. Therefore, CBVw fMRI is a negative contrast that decreases the fMRI signal when blood volumes (i.e., MION concentrations) increase within a voxel. With increasing magnetic field strengths, increased MION concentrations are necessary to counteract the increasing BOLD contributions, which subsequently decrease the baseline signal and functional contrast-to-noise ratio (i.e. sensitivity) through increased susceptibility effects. BOLD contaminations and low baseline signal can be minimized by selecting shorter echo times; while gradient-recalled echo imaging may be better suited than echo-planar imaging to reduce artifacts and signal dropouts associated with the shortened baseline T2* at high magnetic fields (for review, see Kim et al. (2013)). With typical 10 – 15 mg Fe/kg MION doses, the sensitivity of CBVw fMRI was ~1.5 – 2 times greater than GE BOLD at 4.7 – 9.4 T and had peak signal changes in the parenchyma rather than the brain surface (Fig. 1D) (Mandeville and Marota, 1999; Mandeville et al., 1998; Poplawsky and Kim, 2014; Zhao et al., 2005). Many laminar studies (see section 3) show that CBVw fMRI is less sensitive to the dilation of large arterial vessels, especially surface pial vessels, even though large blood volume changes are observed here in studies using optical imaging of intrinsic signal (Kennerley et al., 2005). This can be explained by insufficient SNR caused by the large contrast concentrations and by BOLD contributions large enough to negate the CBV changes in these feeding vessels. This is consistent with a tuning of the fMRI sensitivity toward microvascular compartments and supporting real neurophysiological sources for CBVw fMRI. This is further supported by evidence that the location of peak activation did not change with MION dose (Keilholz et al., 2006; Kim et al., 2013) or whether GE or SE imaging techniques were used with the addition of MION (Fig. 1D–E) (Zhao et al., 2006). Measurements of arterial CBV changes using magnetization transfer-varied arterial spin labeling fMRI were also spatially equivalent to total CBV measurements using MION contrast (Kim et al., 2007), indicating that nonspecific venous CBV changes are small, unless long stimulus durations (Kim and Kim, 2011; Zong et al., 2012) or dexmedetomidine anesthesia are used (Fukuda et al., 2013). Together, contrast-enhanced CBVw fMRI in preclinical models is effective at both increasing the fMRI sensitivity and site-specificity to the layers of the greatest synaptic activity changes (Harel et al., 2006; Kim and Kim, 2010; Lu et al., 2004; Poplawsky et al., 2015; Zhao et al., 2006).

Despite these clear advantages, some caveats should be considered. First, MION-based contrast agents are not approved for clinical MRI applications (approved for iron deficiency treatment only) and is currently reserved for animal study. Therefore, noninvasive CBVw

techniques, like vascular space occupancy (VASO) fMRI-based techniques (Huber et al., 2016; Jin and Kim, 2008b; Lu et al., 2003), can still provide better spatial-specificity compared to GE BOLD but with reduced sensitivity. Also, CBV-weighted signals have BOLD contributions, although relative CBV change maps can be calculated from BOLD and CBVw data (Zhao et al., 2006). Finally, although contrast-enhanced CBVw fMRI reduces contributions from pial and venous vessels, and increases the sensitivity in microvessels, larger penetrating arterioles can still be a source of nonspecific signal contributions. This is of particular importance for laminar studies since these vessels penetrate the layers perpendicularly and can span whole cortical depths, thus confounding more subtle laminar differences. This is especially clear in a recent study comparing the anatomical location of single penetrating venules and arterioles to the GE BOLD and CBVw fMRI signal changes at ultrahigh spatial resolutions (Yu et al., 2016). For a short stimulus duration (<5 s), the largest GE BOLD activations correlated well with the location of emerging venules and CBVw activations with penetrating arterioles (Fig. 2A). However, the relative contributions from nonspecific penetrating arterioles in CBVw fMRI can be reduced with longer stimulation times. Jin and Kim (2008a) compared the specificity of GE BOLD, CBV, and CBF responses and their time dependencies. The early GE BOLD response (Fig. 2B, upper left panel) seems more specific to the middle layer than the late (Fig. 2B, bottom left), as previously described with other fast imaging techniques (Hirano et al., 2011; Silva and Koretsky, 2002; Silva et al., 2000); while the CBVw component is less specific at an earlier time (Fig. 2B, upper right, CBVw only; arrows indicate possible activations in nonspecific penetrating arterioles similar to Fig. 2A) and favors longer stimulation durations (Fig. 2B, right column). Collectively, both CBVw and CBF fMRI are dominated by layer-specific contributions, suggesting that the sum of these components can reduce the GE BOLD response in these same layers.

Although GE BOLD fMRI is the primary tool to study *in vivo* brain activity, its signal sources at laminar resolutions are dominated by nonspecific venous contributions and best serves lower resolution studies. SE BOLD and CBF fMRI methods are better alternatives to GE BOLD at high resolutions in terms of their neural-specificity, but suffer from lower sensitivity and can be more difficult to utilize routinely. On the contrary, CBVw fMRI with intravenous injection of a MION-based contrast agent is, in our opinion, the gold standard for ultrahigh resolution fMRI in basic and preclinical research because of its improved specificity and sensitivity compared to GE BOLD and its ease of implementation.

3. Laminar-specific fMRI

3.1. Neocortex

High-resolution fMRI with different contrasts has been performed to study layer-specific sensory processing in the neocortex. Sensory cortices generally consist of six layers; however, these layers typically function as three. Layer IV contains numerous granule cells (i.e., granular layer) and receives initial synaptic inputs from the thalamus. Sensory stimulation evokes a transient change in neuronal activity first in layer IV and, subsequently, activity spreads immediately into the supragranular (layers I – III) and infragranular (V and VI) layers, and recruits recurrent and feedback circuitry to produce sustained neuronal

activity across all the layers. The supragranular layer then projects to other, higher-order cortices, while the infragranular layer primarily connects with subcortical targets. Thus, in general, sensory evoked neuronal activity consists of initial transient changes, caused by thalamocortical inputs, and is followed by sustained activity caused by the recurrent and feedback inputs. These laminar profiles of specific synaptic events can be obtained by a current source density analysis using electrophysiological measurements obtained at different laminar depths (e.g., (Burns et al., 2010; Sellers et al., 2015)). To fully appreciate laminar fMRI, the relationship between the fMRI signal and this underlying neuronal processing must be understood. Although the exact relationship remains to be elucidated (for review, see Ekstrom (2010)), BOLD signal changes seem to be well correlated to local field potentials (LFPs), particularly the slow fluctuations in the LFP gamma-band (20 – 60 Hz) (Goense and Logothetis, 2008; Logothetis et al., 2001), although it can be context dependent (Maier et al., 2008). Laminar LFP patterns evoked by visual stimulation in the primary visual cortex of anesthetized monkeys show that the power of the sustained gamma-band LFP was high in layer IV and the supragranular layer (Fig. 3A). Since the interlaminar differences may also result from different strengths of initial transient synaptic inputs to individual layers and the initial thalamocortical transient does not seem to have an impact on hemodynamic responses (Harris et al., 2011; Radhakrishnan et al., 2011), the impact of the initial transient input to each layer should be normalized by calculating the ratio of sustained and initial transient responses (Xing et al., 2012) when the laminar LFP power is correlated to the fMRI response. Then, this normalized power of the sustained gamma-band LFP shows the highest value in layer IV (Fig. 3B–C). This highest normalized power of the sustained gamma-band LFP in layer IV also matches the locations of the highest glucose metabolism during stimulation (Kennedy et al., 1976) and the highest capillary density in primate primary visual cortex (Weber et al., 2008). Since changes in blood flow and glucose metabolism accompany changes in neuronal activity (Sokoloff, 1981), the largest fMRI responses evoked by sensory stimulation are expected to also be found in layer IV of the primary sensory cortices, as long as the blood supply to each layer is discretely regulated (Adams et al., 2014).

However, the sensory-stimulation evoked GE BOLD responses have a laminar profile different from this expectation in the primary sensory cortices of anesthetized animals. Typical positive BOLD signal amplitudes decreased from supragranular to infragranular layers (Goense et al., 2012; Harel et al., 2006; Herman et al., 2013; Kennerley et al., 2005; Lu et al., 2004; Silva and Koretsky, 2002; Smirnakis et al., 2007; Zhao et al., 2006). This is likely because BOLD contrast is sensitive to baseline total blood volume (see section 2.1), which is largest at the cortical surface (Tsai et al., 2009). To obtain blood volume changes in microvessels, Harel et al. (2002) measured CBVw fMRI responses in the cortical layers of the cat visual cortex and compared them to BOLD. They found that CBVw signal changes in the middle cortical layer were significantly higher than those in the other layers, unlike BOLD. A similar observation was reported by Lu et al. (2004) in the rat whisker barrel at 3T. In their study, middle layers showing the largest CBVw response contained a dense cFos expression, which indicates large increases in neuronal activity. Later, Harel et al. (2006) histologically confirmed that the maximum CBVw changes occurred in layer IV, while the largest BOLD changes occurred in layer I and the cortical surface by co-registering fMRI

and anatomical MRI maps to the histological images in the cat visual cortex. If CBVw responses reflect total blood volumes, including veins, then CBVw responses should not significantly differ from the BOLD responses. However, CBVw changes predominantly originated from arterioles rather than venous vessels (Kim et al., 2007), indicating an active blood volume regulation. Indeed, arteriole-based CBVw responses were also localized to the cortical middle layer (Kim and Kim, 2010), whereas GE BOLD was not.

To recover layer-specific signals from BOLD responses, several techniques examined ways to remove the nonspecific contributions from large draining veins. By removing voxels containing venous contributions (i.e., the top 40% of activated voxels), layer IV was significantly more active compared to the top and bottom layers in the primate primary visual cortex (Chen et al., 2013). In addition, since the highest GE BOLD signal changes in the large draining veins can be removed with SE techniques (Zhao et al., 2004), Zhao et al. (2006) compared GE and SE BOLD and CBVw fMRI responses in the cat visual cortex at 9.4 T. While they showed that the SE BOLD responses spread almost evenly across all the cortical layers, although the largest surface responses were removed, others showed that the SE BOLD signal peaked both at the surface and the middle layers (Goense and Logothetis, 2006; Goense et al., 2007; Harel et al., 2006). Improved GE BOLD specificity was also observed with fast imaging techniques when responses were mapped before venous draining became prominent. Initially, Silva et al. (2000) obtained dynamic GE BOLD responses of the rat somatosensory cortex with a 108-ms temporal resolution, and found that the middle cortical region had a faster onset time than the cortical surface, indicating that the early positive BOLD response was more specific. Later with an even faster temporal resolution of 40 ms, Silva and Koretsky (2002) confirmed that the fastest onset time of the positive GE BOLD response was in layers IV-V of the rat somatosensory cortex. Similar observations were reported in later studies (Hirano et al., 2011; Jin and Kim, 2008a; Yu et al., 2014). Jin and Kim (2008a) found that the BOLD response in the cat visual cortex was localized to the middle layer at the earliest time (3 – 5 s) and, subsequently, shifted toward the cortical surface (Fig. 2D). Yu et al. (2014) used line scanning fMRI with ~50-ms temporal and ~50-μm spatial resolutions to similarly show that the earliest positive BOLD responses appeared in layer IV for thalamocortical inputs of the rat primary somatosensory cortex (Fig. 3D, red arrow) and layers II/III and V for corticocortical inputs of the motor cortex (Fig. 3D, blue and green arrows). The early onset BOLD specificity was further confirmed by peak MEMRI responses at the same laminar locations (Fig. 3E).

The CBVw responses in the cat visual cortex, on the contrary, appeared in presumably penetrating arterioles at the earliest time (3 – 5 s) and progressively became more localized to the middle layer as the length of the stimulus increased (Fig. 2E) (Jin and Kim, 2008a). These studies seem to suggest that downstream vasodilation follows the upstream vasodilation, although the backpropagation of vasodilation toward upstream vessels was suggested (Iadecola et al., 1997; Tian et al., 2010; Uhlirova et al., 2016). Consistent observations have also been reported in other model systems (Berwick et al., 2008; Moon et al., 2013). This time-dependent CBVw specificity may suggest that active and passive CBV control mechanisms dynamically modulate dilations of different vessel segments (Moon et al., 2013). CBF responses, on the other hand, peaked in the middle cortical layer and its specificity did not change much over time (Jin and Kim, 2008a). With BOLD, CBV and

CBF measures, Herman et al. (2013) estimated $CMRO_2$ between different layers of the rat somatosensory cortex. In their findings, both BOLD and CBV responses decreased from superficial to deep layers, whereas CBF and $CMRO_2$ marked the highest activity in the middle layer; more precisely, they described that “the CBF and LFP patterns were analogous to each other, whereas the $CMRO_2$ and multiple unit activity (MUA) patterns were quite comparable as well”. Although this calibrated BOLD technique may be useful to improve the spatial specificity of fMRI responses, $CMRO_2$ estimates require BOLD, CBV and CBF measurements, and thus it cannot be easily performed. Therefore, these studies imply that CBV and CBF fMRI techniques can mark the highest neuronal activity in layer IV (but see, (Herman et al., 2013; Shih et al., 2013)), while it is difficult to do so with BOLD fMRI alone.

However, the increased specificity of CBV and CBF fMRI does not always seem to be the case. With a ring-shaped checkerboard visual stimulation, Smirnakis et al. (2007) found CBV increases outside of the stimulated region in the primary visual cortex, where BOLD signals were not evoked. Goense et al. (2012) further examined this phenomenon with CBF, CBVw and GE BOLD fMRI at laminar resolutions in the primate primary visual cortex. A ring-shaped checkerboard visual stimulation evoked an increased BOLD signal in the stimulated visual area, whereas it evoked a decreased BOLD signal in the immediately surrounding area that was unstimulated. As in their earlier findings, both CBV and CBF increased in the middle cortical layer, where BOLD signals increased. However, in the region showing the negative BOLD across all the layers, CBV increased in the middle layer, while CBF decreased in the supragranular layer. A negative BOLD response was also evoked by somatosensory stimulation in regions surrounding the stimulated area of the rodent somatosensory cortex (Devor et al., 2007). This surrounding negative BOLD response peaked in the infragranular layer (Boorman et al., 2010; de Celis Alonso et al., 2008) and was accompanied by a decrease in CBF and CBV (Boorman et al., 2010; Devor et al., 2007; Devor et al., 2005). Interestingly, the occurrence of these vascular responses in the surrounding regions was predicted by the passive redistribution of pressure gradients in the vascular network (Boas et al., 2008). However, since neuronal activity was also suppressed in the surrounding region (Devor et al., 2007; Shmuel et al., 2006), inhibitory processes that had increased metabolic activity (Devor et al., 2008; McCasland and Hibbard, 1997; Picard et al., 2013) may possibly be responsible for these responses. However, direct excitation of GABAergic neurons increased CBF response (Anenberg et al., 2015) as well as BOLD and CBVw responses (Poplawsky et al., 2015). Alternatively, neurovascular effects mediated by neuromodulator responses may be involved in this dissociation (Zaldivar et al., 2014). Although it is difficult to reconcile the observations in the negative BOLD regions, nevertheless, at least in the stimulated region where positive BOLD is evoked, CBVw responses are a better indicator for neuronal activity compared to BOLD. However, this largest CBVw response at layer IV evoked by sensory stimulation is insufficient to determine whether fMRI responses accurately represent layer-specific neuronal processing. The CBVw response, instead, could simply reflect the highest capillary density present in layer IV rather than the highest neuronal activity. We recently addressed this concern in the rat olfactory bulb by taking advantage of particular features of its simplified circuitry (Poplawsky et al., 2015).

3.2 Olfactory bulb

A major issue with laminar fMRI is how discrete function in a single layer can be differentiated from activity in the other layers, especially in cortical circuits where neurophysiological activities between layers are reciprocally connected and interdependent. This limits the applicability of laminar fMRI to the study of neuroscience, unless we can better understand how different neurophysiological events contribute to hemodynamic responses and find ways to discreetly and differentially probe circuit function with targeted laminar stimulation. In this regard, the olfactory bulb is an ideal model since fewer recurrent connections between the layers allow for synapses in single discrete layers to be preferentially evoked using different stimuli (Fukuda et al., 2016). This is particularly advantageous to test whether laminar fMRI responses are independent of the baseline blood volume, which is greatest at the surface of the bulb and decreases with bulb depth (Poplawsky et al., 2016; Poplawsky and Kim, 2014). Similarly, the baseline microvascular blood volume is greatest in the synaptic input layer, the superficial glomerular layer (GL), and decreases with bulb depth (Borowsky and Collins, 1989; Lecoq et al., 2009); and matches well with the laminar profile of metabolic demand measured by 2-deoxyglucose (Sharp et al., 1977).

The olfactory bulb consists of six main layers (Fig. 4A) that can be easily identified with endogenous anatomical MRI contrast (Poplawsky et al., 2015; Wei et al., 2016) or MEMRI (Pautler et al., 1998). During odor stimulation, odorant molecules bind to receptors on olfactory receptor neurons (ORNs), located in the olfactory epithelium anterior to the bulb, and evoke action potentials that propagate through unmyelinated axons into the outermost bulb layer, the olfactory nerve layer (ONL). The ORN axon terminals synapse with the apical dendrites of mitral cells (MCs), the primary output neurons of the bulb, within spherical structures called glomeruli in GL that are located immediately below ONL. The MC somas are in the mitral cell layer (MCL) and send their axons to the olfactory cortex via the lateral olfactory tract (LOT). Activity of MCs is modulated by inhibitory granule cells (GCs) through dendrodendritic synapses between the lateral dendrites of MCs and GC dendrites in the external plexiform layer (EPL), which is located between GL and MCL. The GC somas are in the deepest granule cell layer (GCL) and receive inputs from extrinsic feedback projections that travel through the anterior commissure (AC).

A single glomerulus in the olfactory bulb receives projections from only a single population of ORNs that express the same type of odorant receptor. In addition, glomeruli are spatially arranged in distinct anatomical structures so that different odorant molecules elicit unique spatial patterns of glomerular activations throughout the bulb (Rubin and Katz, 1999; Spors and Grinvald, 2002; Uchida et al., 2000). Functional MRI using GE BOLD contrast was first used to map odor-specific activation of glomeruli in coronal sections of the rat olfactory bulb (Xu et al., 2000; Yang et al., 1998) that were consistent with MEMRI (Pautler and Koretsky, 2002) and 2-deoxyglucose (Johnson et al., 1998) activation maps using similar odor stimulations. Later MEMRI studies further observed unique activation maps elicited by different odor stimulations at resolutions capable of distinguishing activity in single glomeruli (Chuang et al., 2010; Chuang et al., 2009), and provided a more direct means of assessing odor-specific synaptic activity with glomerular-resolution MRI technology. During

odor stimulation, the largest BOLD activations were observed in ONL and GL, with little to no BOLD responses in deeper bulb layers. Interestingly, although the odor-evoked fMRI response was largest in GL, evoked LFP amplitude (or gamma power) was largest in GCL where inhibitory neurons reside (Li et al., 2014a); the activity of which is believed to be important for the generation of the gamma frequency oscillation (for review, see Bartos et al. (2007)). To further examine odor-specific activation maps, BOLD responses were evaluated in GL only to form flat maps of glomerular activations and assessed modular activations in the bulb (Xu et al., 2003), similar to previous 2-deoxyglucose analyses (Johnson et al., 2002). Odorants with slightly different carbon chain lengths showed unique BOLD activation patterns, further supporting the use of fMRI for mapping active glomeruli. The pattern of glomerular activity mapped with BOLD was reproducible within and across subjects (Schafer et al., 2006). However, BOLD contrast is complex and is known to be contaminated by vascular changes nonspecific to the site of neuronal activity, such as large changes in draining veins. To examine this, Poplawsky and Kim (2014) compared GE BOLD and CBVw fMRI maps in the same rats. We found that BOLD signal changes were primarily located in the bulb surface vessels, ONL and GL, while CBVw changes peaked in GL and EPL. Activation in ONL may be due to the layer-specific neurovascular coupling of the ORN unmyelinated axons, but few to no capillaries are in this layer and these axons may employ anaerobic respiration for energy (Lecoq et al., 2009). Therefore, the neuronal basis of fMRI responses located in ONL is debatable. Significant activations for both fMRI contrasts were observed in GL, the synaptic input layer, but the location of significant BOLD activations poorly correlated with the sites of CBVw activations; questioning whether either contrast accurately reflected the underlying neuronal activity. Thus, we further examined CBVw and BOLD contrasts while preferentially activating other bulb layers.

Although the greatest layer-specific fMRI responses are primarily observed in input layers (i.e., layer IV of primary visual and somatosensory cortices, GL of the olfactory bulb), these layers also contain the largest baseline microvessel blood volume, which confounds the interpretation of these evoked hemodynamic responses. To test whether fMRI responses accurately reflect synaptic activity in each layer, different layers must be independently evoked. Thus, we measured GE BOLD and CBVw fMRI responses across the bulb layers while we preferentially evoked synaptic activity in GL during natural odor stimulation (5% amyl acetate in mineral oil), EPL during electrical stimulation of LOT, and GCL during electrical stimulation of AC (Fig. 4). The layer-specific neuronal activity is, therefore, independent of the total and microvessel baseline blood volumes, which are greatest at the surface and in GL, respectively, and decrease with depth. We found that the positive BOLD responses were greatest in GL for all three stimulation types, which is likely reflective of the baseline blood volume condition rather than the underlying neuronal activity. On the contrary, the largest CBVw response was discretely segregated to the same layer as the evoked synaptic activity: greatest in GL for odor, EPL for LOT, and GCL for AC stimulations, respectively. Most importantly, despite the least baseline microvessel blood volume in GCL, the CBVw signal changes during AC stimulation were greatest in this layer. These layer-specific fMRI responses that are independent of the baseline blood volume strongly suggest that the microvasculature, particularly blood volume, is regulated within

layers (Poplawsky et al., 2015). More recently, we compared the relationship between the spread of the CBVw laminar response evoked in EPL during stimulation of LOT, and the vascular architecture of this layer using CLARITY-based methods and found a good correspondence between the spread of CBVw signal and the lengths of microvessels (Poplawsky et al., 2016). Therefore, high-resolution fMRI can be used to measure local network activity occurring in individual layers, but caution must be taken when interpreting GE BOLD data.

4. Open questions and future directions

Over the past two decades, many limitations toward examining laminar activity with fMRI have been resolved as discussed previously: 1) local microvessels are specifically regulated by synapses within layers, 2) several fMRI techniques, like contrast-enhanced CBVw fMRI, at laminar resolutions are capable of measuring microvascular changes while mitigating nonspecific vascular contributions, and 3) accurate spatial representations of layer-specific synaptic activity have been demonstrated in various *in vivo* brain circuits. However, there are still outstanding technical and neurophysiological questions that must be addressed to fully appreciate the use of laminar fMRI. How can the temporal and spatial resolutions be improved, with sufficient sensitivity, without compromising the other? How are different types of neuronal populations contributing to the hemodynamic response and can their individual responses be disentangled? What is the exact relationship between direct neurophysiological measurements, such as LFP frequency bands, and layer-specific fMRI responses? Can layer-specific changes be computationally recovered from traditional GE BOLD fMRI? Besides sensory evoked fMRI responses, resting state functional connectivity with fMRI (fcMRI) has useful translations for clinical care (Fox and Greicius, 2010). Interestingly, a study in the primate auditory cortex suggested that sensory evoked responses are initiated in layer IV, while spontaneous activity is initiated in layer V (Sakata and Harris, 2009). Adding laminar information to fcMRI would provide further interest. Despite these questions, laminar fMRI in preclinical models is currently ripe for application, especially with the growing development of transgenic animal models that can be coupled with direct neurophysiological measurements.

Novel developments in data processing may aid in the better deciphering of laminar neuronal activity with fMRI. Currently, general linear models (GLMs) are the mainstream tool to determine fMRI activation maps that compare experimentally acquired time series to predicted responses, which is determined by convolving the rectangular stimulus time course with a generic hemodynamic response function. In their simplest form, GLMs are dependent on temporally-shaped responses that are static across different regions of the brain and are poor at separating specific and nonspecific activity if the temporal characteristics are similar. In our recent work, we evaluated activation maps calculated from a standard GLM and a machine-learning (ML) algorithm using GE BOLD and CBVw fMRI data acquired in our layer-specific olfactory bulb model (Murphy et al., 2016). Compared to the traditional GLM, we found significant improvement of the GE BOLD layer-specificity using ML when it was trained to the expected location of synaptic activity and a map of the total blood volume. This provides intriguing preliminary evidence that latent layer-specific GE BOLD responses can be dissociated from the nonspecific responses. Possibly, when trained to invasive

neurophysiological measurements and detailed maps of the arteries and veins, ML can be an excellent approach to noninvasively estimate laminar synaptic activities from fMRI data alone.

Many of the layer-specific fMRI studies have utilized only a single stimulation condition. One of the intriguing questions is how different stimulations or different contexts can modulate the laminar fMRI response profile. Olman et al. (2012) demonstrated differential layer-specific BOLD activations by preferentially stimulating magnocellular and parvocellular pathways of the visual system, since each pathway is processed in different cortical layers (Livingstone and Hubel, 1988). Specifically, they showed that BOLD responses were highest in superficial layers when the parvocellular pathway was preferentially stimulated, similar to the typical visually-evoked BOLD responses, while it had similar response amplitudes across all layers for the magnocellular preferential stimulation. However, besides neural-specific origins, these observations may also result from strong (1 – 2%) vs. weak (<0.5%) BOLD activations with parvocellular vs. magnocellular preferential stimulations, respectively. Alternatively, Wagner et al. (1981) reported that a moving horizontal grating pattern caused the greatest 2-deoxyglucose uptake in layer IV, while Gaussian visual noise motion increased the uptake in layers II and V more than in layer IV. It would be interesting to determine whether the same conclusions can be drawn from CBVw fMRI to these stimulations. Attentional modulations can also be studied with layer-specific fMRI. For instance, Self et al. (2013) recorded neuronal activity across layers of the primary visual cortex while monkeys performed a figure-ground segregation task. Neuronal activity representing the figure-ground segregation appeared during the sustained activity, such as 100 – 300 ms after stimulus onset. They found that the response was sustained in the superficial layers and particularly in layer V rather than layer IV during this period. Such a late phase modulation would occur by receiving feedbacks from higher-order cortical areas as well as neuromodulator signals, such as acetylcholine, norepinephrine, serotonin, dopamine, and neuropeptides. Therefore, it is interesting to see how the laminar fMRI profiles evoked by a simple sensory stimulation in primary sensory cortex are modulated by remotely stimulating higher cortical areas or neuromodulator nuclei.

Optogenetic tools make dissecting discrete functions of neuronal circuits easier and clean since they target the expression of light-gated ion channels to single neuron types and in specific brain locations (Deisseroth, 2015). Several optogenetic fMRI (ofMRI) studies with the selective expression of channelrhodopsin-2 (ChR2), a cationic channel that depolarizes neurons with blue light, have shown that excitation of ChR2 expressing excitatory or inhibitory neurons increased hemodynamic responses both locally and at their extrinsic targets (Anenberg et al., 2015; Desai et al., 2011; Iordanova et al., 2015; Lee et al., 2010; Li et al., 2014b; Vazquez et al., 2014). ChR2 can also be selectively expressed in specific types of neuromodulatory neurons. For instance, photo-excitation of ChR2 expressing dopaminergic projection neurons originating from the ventral tegmental area, a midbrain nucleus, have been shown to induce BOLD and CBVw responses in regions, such as the striatum and thalamus, that were attenuated by dopamine receptor antagonists (Decot et al., 2017; Ferenczi et al., 2016; Lohani et al., 2017). However, it is currently debatable whether these hemodynamic responses are directly caused by dopaminergic transmission or by

neuromodulation of glutamatergic excitability. In order to best appreciate the use of optogenetic tools in laminar fMRI, direct measurement of evoked neuronal activity must first be measured using techniques like current source density mapping (see section 3) or imaging of genetically-encoded indicators of electrophysiological activity (Lin and Schnitzer, 2016), such as fluorescent calcium indicators. Although these direct approaches have a more focused field of view or are limited to superficial layers, respectively, correlation to direct measurements is essential to authenticate the true laminar fMRI signals from the artifactual (Rungta et al., 2017). In all, ofMRI studies are systematically unlocking the cellular origins of fMRI responses, which are necessary for the accurate interpretation of laminar resolution activation maps. In addition, the ability of ofMRI to target single neuronal populations residing in different layers and having different laminar connections will further aid in the development and application of laminar fMRI. It is then interesting to speculate that laminar fMRI will soon be used to investigate how laminar circuit processing is dysfunctioning in animal models of human diseases or changing under normal learning-induced plasticity.

Acknowledgments

We thank former and current members of our lab, Drs. Tao Jin, Fuqiang Zhao, Tae Kim, and Timothy Duong, for adaptation of their original figures and/or their contributions to laminar fMRI. This work was supported by the National Institutes of Health (NS07391, MH18273, EB003324, and EB018903) and the Institute for Basic Science (IBS-R015-D1).

References

Adams DL, Piserchia V, Economides JR, Horton JC. 2014; Vascular Supply of the Cerebral Cortex is Specialized for Cell Layers but Not Columns. Cereb Cortex. 25(10):3673–3681. [PubMed: 25246513]

Anenberg E, Chan AW, Xie Y, LeDue JM, Murphy TH. 2015; Optogenetic stimulation of GABA neurons can decrease local neuronal activity while increasing cortical blood flow. J Cereb Blood Flow Metab. 35:1579–1586. [PubMed: 26082013]

Attwell D, Buchan AM, Charpak S, Lauritzen M, MacVicar BA, Newman EA. 2010; Glial and neuronal control of brain blood flow. Nature. 468(7321):232–243. [PubMed: 21068832]

Bartos M, Vida I, Jonas P. 2007; Synaptic mechanisms of synchronized gamma oscillations in inhibitory interneuron networks. Nat Rev Neurosci. 8(1):45–56. [PubMed: 17180162]

Berwick J, Johnston D, Jones M, Martindale J, Martin C, Kennerley AJ, Redgrave P, Mayhew JEW. 2008; Fine Detail of Neurovascular Coupling Revealed by Spatiotemporal Analysis of the Hemodynamic Response to Single Whisker Stimulation in Rat Barrel Cortex. J Neurophysiol. 99(2):787–798. [PubMed: 18046008]

Boas DA, Jones SR, Devor A, Huppert TJ, Dale AM. 2008; A vascular anatomical network model of the spatio-temporal response to brain activation. Neuroimage. 40(3):1116–1129. [PubMed: 18289880]

Boorman L, Kennerley AJ, Johnston D, Jones M, Zheng Y, Redgrave P, Berwick J. 2010; Negative Blood Oxygen Level Dependence in the Rat: A Model for Investigating the Role of Suppression in Neurovascular Coupling. J Neurosci. 30(12):4285–4294. [PubMed: 20335464]

Borowsky IW, Collins RC. 1989; Metabolic anatomy of brain: A comparison of regional capillary density, glucose metabolism, and enzyme activities. J Comp Neurol. 288(3):401–413. [PubMed: 2551935]

Boxerman JL, Hamberg LM, Rosen BR, Weisskoff RM. 1995; MR contrast due to intravascular magnetic susceptibility perturbations. Magn Reson Med. 34(4):555–566. [PubMed: 8524024]

Burns SP, Xing D, Shapley RM. 2010; Comparisons of the Dynamics of Local Field Potential and Multiunit Activity Signals in Macaque Visual Cortex. J Neurosci. 30(41):13739–13749. [PubMed: 20943914]

Chen G, Wang F, Gore JC, Roe AW. 2013; Layer-specific BOLD activation in awake monkey V1 revealed by ultra-high spatial resolution functional magnetic resonance imaging. Neuroimage. 64:147–155. [PubMed: 22960152]

Chen JJ, Pike GB. 2009; Origins of the BOLD post-stimulus undershoot. Neuroimage. 46(3):559–568. [PubMed: 19303450]

Chuang K-H, Belluscio L, Koretsky AP. 2010; In vivo detection of individual glomeruli in the rodent olfactory bulb using manganese enhanced MRI. Neuroimage. 49(2):1350–1356. [PubMed: 19800011]

Chuang K-H, Lee JH, Silva AC, Belluscio L, Koretsky AP. 2009; Manganese enhanced MRI reveals functional circuitry in response to odorant stimuli. Neuroimage. 44(2):363–372. [PubMed: 18848997]

de Celis Alonso B, Lowe AS, Dear JP, Lee KC, Williams SCR, Finnerty GT. 2008; Sensory Inputs from Whisking Movements Modify Cortical Whisker Maps Visualized with Functional Magnetic Resonance Imaging. Cereb Cortex. 18(6):1314–1325. [PubMed: 17951597]

Decot HK, Namboodiri VMK, Gao W, McHenry JA, Jennings JH, Lee S-H, Kantak PA, Jill Kao Y-C, Das M, Witten IB, Deisseroth K, Shih Y-YI, Stuber GD. 2017; Coordination of Brain-Wide Activity Dynamics by Dopaminergic Neurons. Neuropsychoparmacol. 42(3):615–627.

Deisseroth K. 2015; Optogenetics: 10 years of microbial opsins in neuroscience. Nat Neurosci. 18(9): 1213–1225. [PubMed: 26308982]

Desai M, Kahn I, Knoblich U, Bernstein J, Atallah H, Yang A, Kopell N, Buckner RL, Graybiel AM, Moore CI, Boyden ES. 2011; Mapping brain networks in awake mice using combined optical neural control and fMRI. J Neurophysiol. 105(3):1393–1405. [PubMed: 21160013]

Detre JA, Leigh JS, Williams DS, Koretsky AP. 1992; Perfusion imaging. Magn Reson Med. 23(1):37–45. [PubMed: 1734182]

Devor A, Hillman EMC, Tian P, Waeber C, Teng IC, Ruvinskaya L, Shalinsky MH, Zhu H, Haslinger RH, Narayanan SN, Ulbert I, Dunn AK, Lo EH, Rosen BR, Dale AM, Kleinfeld D, Boas DA. 2008; Stimulus-Induced Changes in Blood Flow and 2-Deoxyglucose Uptake Dissociate in Ipsilateral Somatosensory Cortex. J Neurosci. 28(53):14347–14357. [PubMed: 19118167]

Devor A, Tian P, Nishimura N, Teng IC, Hillman EMC, Narayanan SN, Ulbert I, Boas DA, Kleinfeld D, Dale AM. 2007; Suppressed Neuronal Activity and Concurrent Arteriolar Vasoconstriction May Explain Negative Blood Oxygenation Level-Dependent Signal. J Neurosci. 27(16):4452–4459. [PubMed: 17442830]

Devor A, Ulbert I, Dunn AK, Narayanan SN, Jones SR, Andermann ML, Boas DA, Dale AM. 2005; Coupling of the cortical hemodynamic response to cortical and thalamic neuronal activity. Proc Natl Acad Sci U S A. 102(10):3822–3827. [PubMed: 15734797]

Duong TQ, Kim D-S, Uğurbil K, Kim S-G. 2001; Localized cerebral blood flow response at submillimeter columnar resolution. Proc Natl Acad Sci U S A. 98(19):10904–10909. [PubMed: 11526212]

Duong TQ, Kim DS, Ugurbil K, Kim SG. 2000a; Spatiotemporal dynamics of the BOLD fMRI signals: toward mapping submillimeter cortical columns using the early negative response. Magn Reson Med. 44(2):231–242. [PubMed: 10918322]

Duong TQ, Silva AC, Lee SP, Kim SG. 2000b; Functional MRI of calcium-dependent synaptic activity: cross correlation with CBF and BOLD measurements. Magn Reson Med. 43(3):383–392. [PubMed: 10725881]

Ekstrom A. 2010; How and when the fMRI BOLD signal relates to underlying neural activity: The danger in dissociation. Brain Res Rev. 62(2):233–244. [PubMed: 20026191]

Ernst T, Hennig J. 1994; Observation of a Fast Response in Functional MR. Magn Reson Med. 32(1): 146–149. [PubMed: 8084231]

Ferenczi EA, Zalocusky KA, Liston C, Grosenick L, Warden MR, Amatya D, Katovich K, Mehta H, Patenaude B, Ramakrishnan C, Kalanithi P, Etkin A, Knutson B, Glover GH, Deisseroth K. 2016;

Prefrontal cortical regulation of brainwide circuit dynamics and reward-related behavior. Science. 351(6268):aac9698. [PubMed: 26722001]

Fernández-Klett F, Offenhauser N, Dirnagl U, Priller J, Lindauer U. 2010; Pericytes in capillaries are contractile in vivo, but arterioles mediate functional hyperemia in the mouse brain. Proc Natl Acad Sci U S A. 107(51):22290–22295. [PubMed: 21135230]

Fox M, Greicius M. 2010; Clinical applications of resting state functional connectivity. Front Syst Neurosci. 4(19):1–13. [PubMed: 20204156]

Fukuda, M, Poplawsky, AJ, Kim, S-G. Chapter 6 - Submillimeter-resolution fMRI: Toward understanding local neural processing. In: Kazuto Masamoto, HH, Katsuya, Y, editors. Progress in Brain Research. Elsevier; 2016. 123–152.

Fukuda M, Vazquez AL, Zong X, Kim SG. 2013; Effects of the alpha(2)-adrenergic receptor agonist dexmedetomidine on neural, vascular and BOLD fMRI responses in the somatosensory cortex. Eur J Neurosci. 37(1):80–95. [PubMed: 23106361]

Gagnon L, Sakadžić S, Lesage F, Musacchia JJ, Lefebvre J, Fang Q, Yücel MA, Evans KC, Mandeville ET, Cohen-Adad J, Polimeni JaR, Yaseen MA, Lo EH, Greve DN, Buxton RB, Dale AM, Devor A, Boas DA. 2015; Quantifying the Microvascular Origin of BOLD-fMRI from First Principles with Two-Photon Microscopy and an Oxygen-Sensitive Nanoprobe. J Neurosci. 35(8): 3663–3675. [PubMed: 25716864]

Goense J, Merkle H, Logothetis NK. 2012; High-Resolution fMRI Reveals Laminar Differences in Neurovascular Coupling between Positive and Negative BOLD Responses. Neuron. 76(3):629–639. [PubMed: 23141073]

Goense JBM, Logothetis NK. 2006; Laminar specificity in monkey V1 using high-resolution SE-fMRI. Magn Reson Imaging. 24(4):381–392. [PubMed: 16677944]

Goense JBM, Logothetis NK. 2008; Neurophysiology of the BOLD fMRI Signal in Awake Monkeys. Curr Biol. 18(9):631–640. [PubMed: 18439825]

Goense JBM, Zappe A-C, Logothetis NK. 2007; High-resolution fMRI of macaque V1. Magn Reson Imaging. 25(6):740–747. [PubMed: 17499466]

Hall CN, Reynell C, Gesslein B, Hamilton NB, Mishra A, Sutherland BA, O'Farrell FM, Buchan AM, Lauritzen M, Attwell D. 2014; Capillary pericytes regulate cerebral blood flow in health and disease. Nature. 508(7494):55–60. [PubMed: 24670647]

Harel N, Lin J, Moeller S, Ugurbil K, Yacoub E. 2006; Combined imaging–histological study of cortical laminar specificity of fMRI signals. Neuroimage. 29(3):879–887. [PubMed: 16194614]

Harel, N; Zhao, F; Wang, P; Kim, S-G. Cortical layer specificity of BOLD and CBV fMRI signals at ultra-high resolution. Program No. 9. Proc 10th Annual Meeting; Honolulu, HI: ISMRM; 2002.

Harris JJ, Reynell C, Attwell D. 2011; The physiology of developmental changes in BOLD functional imaging signals. Dev Cogn Neurosci. 1(3):199–216. [PubMed: 22436508]

Herman P, Sanganahalli BG, Blumenfeld H, Rothman DL, Hyder F. 2013; Quantitative basis for neuroimaging of cortical laminae with calibrated functional MRI. Proc Natl Acad Sci U S A. 110(37):15115–15120. [PubMed: 23980158]

Hill RA, Tong L, Yuan P, Murikinati S, Gupta S, Grutzendler J. 2015; Regional Blood Flow in the Normal and Ischemic Brain Is Controlled by Arteriolar Smooth Muscle Cell Contractility and Not by Capillary Pericytes. Neuron. 87(1):95–110. [PubMed: 26119027]

Hirano Y, Stefanovic B, Silva AC. 2011; Spatiotemporal Evolution of the Functional Magnetic Resonance Imaging Response to Ultrashort Stimuli. J Neurosci. 31(4):1440–1447. [PubMed: 21273428]

Hu X, Yacoub E. 2012; The story of the initial dip in fMRI. Neuroimage. 62(2):1103–1108. [PubMed: 22426348]

Hua J, Stevens RD, Huang AJ, Pekar JJ, van Zijl PCM. 2011; Physiological origin for the BOLD poststimulus undershoot in human brain: vascular compliance versus oxygen metabolism. J Cereb Blood Flow Metab. 31(7):1599–1611. [PubMed: 21468090]

Huber L, Goense J, Kennerley AJ, Trampel R, Guidi M, Reimer E, Ivanov D, Neef N, Gauthier CJ, Turner R, Möller HE. 2015; Cortical lamina-dependent blood volume changes in human brain at 7 T. Neuroimage. 107:23–33. [PubMed: 25479018]

Huber L, Ivanov D, Handwerker DA, Marrett S, Guidi M, Uludağ K, Bandettini PA, Poser BA. 2016Techniques for blood volume fMRI with VASO: From low-resolution mapping towards sub-millimeter layer-dependent applications. Neuroimage. 10.1016/j.neuroimage.2016.11.039

Iadecola C, Yang G, Ebner TJ, Chen G. 1997; Local and Propagated Vascular Responses Evoked by Focal Synaptic Activity in Cerebellar Cortex. J Neurophysiol. 78(2):651–659. [PubMed: 9307102]

Iordanova B, Vazquez AL, Poplawsky AJ, Fukuda M, Kim S-G. 2015; Neural and hemodynamic responses to optogenetic and sensory stimulation in the rat somatosensory cortex. J Cereb Blood Flow Metab. 35(6):922–932. [PubMed: 25669905]

Jezzard P, Rauschecker JP, Malonek D. 1997; An in vivo model for functional MRI in cat visual cortex. Magn Reson Med. 38(5):699–705. [PubMed: 9358442]

Jin T, Kim S-G. 2008a; Cortical layer-dependent dynamic blood oxygenation, cerebral blood flow and cerebral blood volume responses during visual stimulation. Neuroimage. 43(1):1–9. [PubMed: 18655837]

Jin T, Kim S-G. 2008b; Improved cortical-layer specificity of vascular space occupancy fMRI with slab inversion relative to spin-echo BOLD at 9.4 T. Neuroimage. 40(1):59–67. [PubMed: 18249010]

Johnson BA, Ho SL, Xu Z, Yihan JS, Yip S, Hingco EE, Leon M. 2002; Functional mapping of the rat olfactory bulb using diverse odorants reveals modular responses to functional groups and hydrocarbon structural features. J Comp Neurol. 449(2):180–194. [PubMed: 12115688]

Johnson BA, Woo CC, Leon M. 1998; Spatial coding of odorant features in the glomerular layer of the rat olfactory bulb. J Comp Neurol. 393(4):457–471. [PubMed: 9550151]

Keilholz SD, Silva AC, Raman M, Merkle H, Koretsky AP. 2006; BOLD and CBV-weighted functional magnetic resonance imaging of the rat somatosensory system. Magn Reson Med. 55(2): 316–324. [PubMed: 16372281]

Kennedy C, Des Rosiers MH, Sakurada O, Shinohara M, Reivich M, Jehle JW, Sokoloff L. 1976; Metabolic mapping of the primary visual system of the monkey by means of the autoradiographic [14C]deoxyglucose technique. Proc Natl Acad Sci U S A. 73(11):4230–4234. [PubMed: 825861]

Kennerley AJ, Berwick J, Martindale J, Johnston D, Papadakis N, Mayhew JE. 2005; Concurrent fMRI and optical measures for the investigation of the hemodynamic response function. Magn Reson Med. 54(2):354–365. [PubMed: 16032695]

Kim DS, Duong TQ, Kim SG. 2000; High-resolution mapping of iso-orientation columns by fMRI. Nat Neurosci. 3(2):164–169. [PubMed: 10649572]

Kim S-G. 1995; Quantification of relative cerebral blood flow change by flow-sensitive alternating inversion recovery (FAIR) technique: Application to functional mapping. Magn Reson Med. 34(3): 293–301. [PubMed: 7500865]

Kim S-G, Harel N, Jin T, Kim T, Lee P, Zhao F. 2013; Cerebral blood volume MRI with intravascular superparamagnetic iron oxide nanoparticles. NMR Biomed. 26:949–962. [PubMed: 23208650]

Kim S-G, Ogawa S. 2012; Biophysical and physiological origins of blood oxygenation level-dependent fMRI signals. J Cereb Blood Flow Metab. 32(7):1188–1206. [PubMed: 22395207]

Kim T, Hendrich KS, Masamoto K, Kim S-G. 2007; Arterial versus total blood volume changes during neural activity-induced cerebral blood flow change: implication for BOLD fMRI. J Cereb Blood Flow Metab. 27(6):1235–1247. [PubMed: 17180136]

Kim T, Kim S-G. 2010; Cortical layer-dependent arterial blood volume changes: Improved spatial specificity relative to BOLD fMRI. Neuroimage. 49(2):1340–1349. [PubMed: 19800013]

Kim T, Kim S-G. 2011; Temporal dynamics and spatial specificity of arterial and venous blood volume changes during visual stimulation: implication for BOLD quantification. J Cereb Blood Flow Metab. 31(5):1211–1222. [PubMed: 21179068]

Kisler K, Nelson AR, Rege SV, Ramanathan A, Wang Y, Ahuja A, Lazic D, Tsai PS, Zhao Z, Zhou Y, Boas DA, Sakadzic S, Zlokovic BV. 2017; Pericyte degeneration leads to neurovascular uncoupling and limits oxygen supply to brain. Nat Neurosci. doi: 10.1038/nn.4489

Koopmans PJ, Barth M, Norris DG. 2010; Layer-specific BOLD activation in human V1. Hum Brain Mapp. 31(9):1297–1304. [PubMed: 20082333]

Kwong KK, Chesler DA, Weisskoff RM, Donahue KM, Davis TL, Ostergaard L, Campbell TA, Rosen BR. 1995; MR perfusion studies with T1-weighted echo planar imaging. Magn Reson Med. 34(6): 878–887. [PubMed: 8598815]

Lecoq J, Tiret P, Najac M, Shepherd GM, Greer CA, Charpak S. 2009; Odor-Evoked Oxygen Consumption by Action Potential and Synaptic Transmission in the Olfactory Bulb. J Neurosci. 29(5):1424–1433. [PubMed: 19193889]

Lee JH, Durand R, Gradinaru V, Zhang F, Goshen I, Kim D-S, Fenno LE, Ramakrishnan C, Deisseroth K. 2010; Global and local fMRI signals driven by neurons defined optogenetically by type and wiring. Nature. 465(7299):788–792. [PubMed: 20473285]

Lee S-P, Silva AC, Ugurbil K, Kim S-G. 1999; Diffusion-weighted spin-echo fMRI at 9.4 T: Microvascular/tissue contribution to BOLD signal changes. Magn Reson Med. 42(5):919–928. [PubMed: 10542351]

Li B, Gong L, Wu R, Li A, Xu F. 2014a; Complex relationship between BOLD-fMRI and electrophysiological signals in different olfactory bulb layers. Neuroimage. 95:29–38. [PubMed: 24675646]

Li N, van Zijl P, Thakor N, Pelled G. 2014b; Study of the Spatial Correlation Between Neuronal Activity and BOLD fMRI Responses Evoked by Sensory and Channelrhodopsin-2 Stimulation in the Rat Somatosensory Cortex. J Mol Neurosci. 53(4):553–561. [PubMed: 24443233]

Lin MZ, Schnitzer MJ. 2016; Genetically encoded indicators of neuronal activity. Nat Neurosci. 19(9): 1142–1153. [PubMed: 27571193]

Lin Y-J, Koretsky AP. 1997; Manganese ion enhances T1-weighted MRI during brain activation: An approach to direct imaging of brain function. Magn Reson Med. 38(3):378–388. [PubMed: 9339438]

Livingstone M, Hubel D. 1988; Segregation of form, color, movement, and depth: anatomy, physiology, and perception. Science. 240(4853):740–749. [PubMed: 3283936]

Logothetis NK, Pauls J, Augath M, Trinath T, Oeltermann A. 2001; Neurophysiological investigation of the basis of the fMRI signal. Nature. 412(6843):150–157. [PubMed: 11449264]

Lohani S, Poplawsky AJ, Kim S-G, Moghaddam B. 2017; Unexpected global impact of VTA dopamine neuron activation as measured by opto-fMRI. Mol Psychiatr. 22:585–594.

Lu H, Golay X, Pekar JJ, Van Zijl PC. 2003; Functional magnetic resonance imaging based on changes in vascular space occupancy. Magn Reson Med. 50(2):263–274. [PubMed: 12876702]

Lu H, Patel S, Luo F, Li S-J, Hillard CJ, Ward BD, Hyde JS. 2004; Spatial correlations of laminar BOLD and CBV responses to rat whisker stimulation with neuronal activity localized by Fos expression. Magn Reson Med. 52(5):1060–1068. [PubMed: 15508149]

Maier A, Wilke M, Aura C, Zhu C, Ye FQ, Leopold DA. 2008; Divergence of fMRI and neural signals in V1 during perceptual suppression in the awake monkey. Nat Neurosci. 11(10):1193–1200. [PubMed: 18711393]

Malonek D, Grinvald A. 1996; Interactions between electrical activity and cortical microcirculation revealed by imaging spectroscopy: implications for functional brain mapping. Science. 272(5261): 551–554. [PubMed: 8614805]

Mandeville JB, Jenkins BG, Chen Y-CI, Choi J-K, Kim YR, Belen D, Liu C, Kosofsky BE, Marota JJA. 2004; Exogenous contrast agent improves sensitivity of gradient-echo functional magnetic resonance imaging at 9.4 T. Magn Reson Med. 52(6):1272–1281. [PubMed: 15562489]

Mandeville JB, Marota JJA. 1999; Vascular filters of functional MRI: Spatial localization using BOLD and CBV contrast. Magn Reson Med. 42(3):591–598. [PubMed: 10467305]

Mandeville JB, Marota JJA, Ayata C, Zaharchuk G, Moskowitz MA, Rosen BR, Weisskoff RM. 1999; Evidence of a Cerebrovascular Postarteriole Windkessel with Delayed Compliance. J Cereb Blood Flow Metab. 19(6):679–689. [PubMed: 10366199]

Mandeville JB, Marota JJA, Kosofsky BE, Keltner JR, Weissleder R, Rosen BR, Weisskoff RM. 1998; Dynamic functional imaging of relative cerebral blood volume during rat forepaw stimulation. Magn Reson Med. 39(4):615–624. [PubMed: 9543424]

Markuerkiaga I, Barth M, Norris DG. 2016; A cortical vascular model for examining the specificity of the laminar BOLD signal. Neuroimage. 132:491–498. [PubMed: 26952195]

McCasland JS, Hibbard LS. 1997; GABAergic Neurons in Barrel Cortex Show Strong, Whisker-Dependent Metabolic Activation during Normal Behavior. J Neurosci. 17(14):5509–5527. [PubMed: 9204933]

Mishra A, Reynolds JP, Chen Y, Gourine AV, Rusakov DA, Attwell D. 2016; Astrocytes mediate neurovascular signaling to capillary pericytes but not to arterioles. Nat Neurosci. 19(12):1619–1627. [PubMed: 27775719]

Moon C-H, Fukuda M, Park S-H, Kim S-G. 2007; Neural Interpretation of Blood Oxygenation Level-Dependent fMRI Maps at Submillimeter Columnar Resolution. J Neurosci. 27(26):6892–6902. [PubMed: 17596437]

Moon CH, Fukuda M, Kim S-G. 2013; Spatiotemporal characteristics and vascular sources of neural-specific and -nonspecific fMRI signals at submillimeter columnar resolution. Neuroimage. 64:91–103. [PubMed: 22960251]

Murphy MC, Poplawsky AJ, Vazquez AL, Chan KC, Kim S-G, Fukuda M. 2016; Improved spatial accuracy of functional maps in the rat olfactory bulb using supervised machine learning approach. Neuroimage. 137:1–8. [PubMed: 27236085]

Ogawa S, Lee TM, Kay AR, Tank DW. 1990; Brain Magnetic Resonance Imaging with Contrast Dependent on Blood Oxygenation. Proc Natl Acad Sci U S A. 87(24):9868–9872. [PubMed: 2124706]

Ogawa S, Menon R, Kim S-G, Ugurbil K. 1998; On the Characteristics of Functional Magnetic Resonance Imaging of the Brain. Annu Rev Bioph Biom. 27(1):447–474.

Ogawa S, Tank DW, Menon R, Ellermann JM, Kim SG, Merkle H, Ugurbil K. 1992; Intrinsic signal changes accompanying sensory stimulation: functional brain mapping with magnetic resonance imaging. Proc Natl Acad Sci U S A. 89(13):5951–5955. [PubMed: 1631079]

Olman CA, Harel N, Feinberg DA, He S, Zhang P, Ugurbil K, Yacoub E. 2012; Layer-Specific fMRI Reflects Different Neuronal Computations at Different Depths in Human V1. PLoS One. 7(3):e32536. [PubMed: 22448223]

Pautler RG, Koretsky AP. 2002; Tracing Odor-Induced Activation in the Olfactory Bulbs of Mice Using Manganese-Enhanced Magnetic Resonance Imaging. Neuroimage. 16(2):441–448. [PubMed: 12030829]

Pautler RG, Silva AC, Koretsky AP. 1998; In vivo neuronal tract tracing using manganese-enhanced magnetic resonance imaging. Magn Reson Med. 40(5):740–748. [PubMed: 9797158]

Picard N, Matsuzaka Y, Strick PL. 2013; Extended practice of a motor skill is associated with reduced metabolic activity in M1. Nat Neurosci. 16(9):1340–1347. [PubMed: 23912947]

Polimeni JR, Fischl B, Greve DN, Wald LL. 2010; Laminar analysis of 7T BOLD using an imposed spatial activation pattern in human V1. Neuroimage. 52(4):1334–1346. [PubMed: 20460157]

Poplawsky, AJ; Fukuda, M; Kang, B-m; Kim, JH; Chung, K; Suh, M; Kim, S-G. Vascular architecture with CLARITY suggests that contrast-enhanced high-resolution fMRI is dominated by microvessel dilation. Program No. 632.10. Society for Neuroscience; San Diego, CA. 2016.

Poplawsky AJ, Fukuda M, Murphy M, Kim S-G. 2015; Layer-Specific fMRI Responses to Excitatory and Inhibitory Neuronal Activities in the Olfactory Bulb. J Neurosci. 35(46):15263–15275. [PubMed: 26586815]

Poplawsky AJ, Kim S-G. 2014; Layer-dependent BOLD and CBV-weighted fMRI responses in the rat olfactory bulb. Neuroimage. 91:237–251. [PubMed: 24418506]

Radhakrishnan H, Wu W, Boas D, Franceschini MA. 2011; Study of neurovascular coupling by modulating neuronal activity with GABA. Brain Res. 1372:1–12. [PubMed: 21145313]

Ress D, Glover GH, Liu J, Wandell B. 2007; Laminar profiles of functional activity in the human brain. Neuroimage. 34(1):74–84. [PubMed: 17011213]

Rubin BD, Katz LC. 1999; Optical Imaging of Odorant Representations in the Mammalian Olfactory Bulb. Neuron. 23(3):499–511. [PubMed: 10433262]

Rungta RL, Osmanski B-F, Boido D, Tanter M, Charpak S. 2017; Light controls cerebral blood flow in naive animals. Nat Commun. 8:14191. [PubMed: 28139643]

Sakamoto M, Kageyama R, Imayoshi I. 2014; The functional significance of newly born neurons integrated into olfactory bulb circuits. Front Neurosci. 8(121)

Sakata S, Harris KD. 2009; Laminar structure of spontaneous and sensory-evoked population activity in auditory cortex. Neuron. 64(3):404–418. [PubMed: 19914188]

Schafer JR, Kida I, Xu F, Rothman DL, Hyder F. 2006; Reproducibility of odor maps by fMRI in rodents. Neuroimage. 31(3):1238–1246. [PubMed: 16632382]

Self MW, van Kerkoerle T, Super H, Roelfsema PR. 2013; Distinct roles of the cortical layers of area V1 in figure-ground segregation. Curr Biol. 23(21):2121–2129. [PubMed: 24139742]

Sellers KK, Bennett DV, Hutt A, Williams JH, Fröhlich F. 2015; Awake vs. anesthetized: layer-specific sensory processing in visual cortex and functional connectivity between cortical areas. J Neurophysiol. 113(10):3798–3815. [PubMed: 25833839]

Sharp FR, Kauer JS, Shepherd GM. 1977; Laminar analysis of 2-deoxyglucose uptake in olfactory bulb and olfactory cortex of rabbit and rat. J Neurophysiol. 40(4):800–813. [PubMed: 886371]

Shih Y-YI, Chen Y-Y, Lai H-Y, Kao Y-CJ, Shyu B-C, Duong TQ. 2013; Ultra high-resolution fMRI and electrophysiology of the rat primary somatosensory cortex. Neuroimage. 73:113–120. [PubMed: 23384528]

Shmuel A, Augath M, Oeltermann A, Logothetis NK. 2006; Negative functional MRI response correlates with decreases in neuronal activity in monkey visual area V1. Nat Neurosci. 9(4):569–577. [PubMed: 16547508]

Silva AC. 2012; Using manganese-enhanced MRI to understand BOLD. Neuroimage. 62(2):1009–1013. [PubMed: 22245640]

Silva AC, Kim S-G. 1999; Pseudo-continuous arterial spin labeling technique for measuring CBF dynamics with high temporal resolution. Magn Reson Med. 42(3):425–429. [PubMed: 10467285]

Silva AC, Koretsky AP. 2002; Laminar specificity of functional MRI onset times during somatosensory stimulation in rat. Proc Natl Acad Sci U S A. 99(23):15182–15187. [PubMed: 12407177]

Silva AC, Lee SP, Iadecola C, Kim SG. 2000; Early temporal characteristics of cerebral blood flow and deoxyhemoglobin changes during somatosensory stimulation. J Cereb Blood Flow Metab. 20(1):201–206. [PubMed: 10616809]

Sirotin YB, Hillman EMC, Bordier C, Das A. 2009; Spatiotemporal precision and hemodynamic mechanism of optical point spreads in alert primates. Proc Natl Acad Sci U S A. 106(43):18390–18395. [PubMed: 19828443]

Smirnakis SM, Schmid MC, Weber B, Tolias AS, Augath M, Logothetis NK. 2007; Spatial Specificity of BOLD versus Cerebral Blood Volume fMRI for Mapping Cortical Organization. J Cereb Blood Flow Metab. 27(6):1248–1261. [PubMed: 17213863]

Sokoloff L. 1981; Relationships among local functional activity, energy metabolism, and blood flow in the central nervous system. Fed Proc. 40(8):2311–2316. [PubMed: 7238911]

Spors H, Grinvald A. 2002; Spatio-Temporal Dynamics of Odor Representations in the Mammalian Olfactory Bulb. Neuron. 34(2):301–315. [PubMed: 11970871]

Thompson JK, Peterson MR, Freeman RD. 2003; Single-neuron activity and tissue oxygenation in the cerebral cortex. Science. 299(5609):1070–1072. [PubMed: 12586942]

Tian P, Teng IC, May LD, Kurz R, Lu K, Scadeng M, Hillman EMC, De Crespigny AJ, D'Arceuil HE, Mandeville JB, Marota JJA, Rosen BR, Liu TT, Boas DA, Buxton RB, Dale AM, Devor A. 2010; Cortical depth-specific microvascular dilation underlies laminar differences in blood oxygenation level-dependent functional MRI signal. Proc Natl Acad Sci U S A. 107(34):15246–15251. [PubMed: 20696904]

Tsai PS, Kaufhold JP, Blinder P, Friedman B, Drew PJ, Karten HJ, Lyden PD, Kleinfeld D. 2009; Correlations of Neuronal and Microvascular Densities in Murine Cortex Revealed by Direct Counting and Colocalization of Nuclei and Vessels. J Neurosci. 29(46):14553–14570. [PubMed: 19923289]

Uchida N, Takahashi YK, Tanifuji M, Mori K. 2000; Odor maps in the mammalian olfactory bulb: domain organization and odorant structural features. Nat Neurosci. 3(10):1035–1043. [PubMed: 11017177]

Uhlirova H, et al. 2016; Cell type specificity of neurovascular coupling in cerebral cortex. eLife. 5:e14315. [PubMed: 27244241]

van Zijl PCM, Hua J, Lu H. 2012; The BOLD post-stimulus undershoot, one of the most debated issues in fMRI. Neuroimage. 62(2):1092–1102. [PubMed: 22248572]

Vanzetta I, Grinvald A. 1999; Increased Cortical Oxidative Metabolism Due to Sensory Stimulation: Implications for Functional Brain Imaging. Science. 286(5444):1555–1558. [PubMed: 10567261]

Vazquez AL, Fukuda M, Crowley JC, Kim S-G. 2014; Neural and Hemodynamic Responses Elicited by Forelimb- and Photo-stimulation in Channelrhodopsin-2 Mice: Insights into the Hemodynamic Point Spread Function. Cereb Cortex. 24(11):2908–2919. [PubMed: 23761666]

Wagner HJ, Hoffmann KP, Zwerger H. 1981; Layer-specific labelling of cat visual cortex after stimulation with visual noise: a [3H]2-deoxy-d-glucose study. Brain Res. 224(1):31–43. [PubMed: 7284839]

Weber B, Keller AL, Reichold J, Logothetis NK. 2008; The microvascular system of the striate and extrastriate visual cortex of the macaque. Cereb Cortex. 18(10):2318–2330. [PubMed: 18222935]

Wei H, Xie L, Dibb R, Li W, Decker K, Zhang Y, Johnson GA, Liu C. 2016; Imaging whole-brain cytoarchitecture of mouse with MRI-based quantitative susceptibility mapping. Neuroimage. 137:107–115. [PubMed: 27181764]

Weisskoff RM, Zuo CS, Boxerman JL, Rosen BR. 1994; Microscopic susceptibility variation and transverse relaxation: theory and experiment. Magn Reson Med. 31(6):601–610. [PubMed: 8057812]

Xing D, Yeh C-I, Burns S, Shapley RM. 2012; Laminar analysis of visually evoked activity in the primary visual cortex. Proc Natl Acad Sci U S A. 109(34):13871–13876. [PubMed: 22872866]

Xu F, Kida I, Hyder F, Shulman RG. 2000; Assessment and discrimination of odor stimuli in rat olfactory bulb by dynamic functional MRI. Proc Natl Acad Sci U S A. 97(19):10601–10606. [PubMed: 10973488]

Xu F, Liu N, Kida I, Rothman DL, Hyder F, Shepherd GM. 2003; Odor maps of aldehydes and esters revealed by functional MRI in the glomerular layer of the mouse olfactory bulb. Proc Natl Acad Sci U S A. 100(19):11029–11034. [PubMed: 12963819]

Yang X, Renken R, Hyder F, Siddeek M, Greer CA, Shepherd GM, Shulman RG. 1998; Dynamic mapping at the laminar level of odor-elicited responses in rat olfactory bulb by functional MRI. Proc Natl Acad Sci U S A. 95(13):7715–7720. [PubMed: 9636216]

Yu X, He Y, Wang M, Merkle H, Dodd SJ, Silva AC, Koretsky AP. 2016; Sensory and optogenetically driven single-vessel fMRI. Nat Meth. 13(4):337–340.

Yu X, Qian C, Chen D-y, Dodd SJ, Koretsky AP. 2014; Deciphering laminar-specific neural inputs with line-scanning fMRI. Nat Methods. 11(1):55–58. [PubMed: 24240320]

Zaldivar D, Rauch A, Whittingstall K, Logothetis Nikos K, Goense J. 2014; Dopamine-Induced Dissociation of BOLD and Neural Activity in Macaque Visual Cortex. Curr Biol. 24(23):2805–2811. [PubMed: 25456449]

Zappe AC, Pfeuffer J, Merkle H, Logothetis NK, Goense JB. 2008; The Effect of Labeling Parameters on Perfusion-Based fMRI in Nonhuman Primates. J Cereb Blood Flow Metab. 28(3):640–652. [PubMed: 17960143]

Zhao F, Jin T, Wang P, Kim S-G. 2007; Improved spatial localization of post-stimulus BOLD undershoot relative to positive BOLD. Neuroimage. 34(3):1084–1092. [PubMed: 17161623]

Zhao F, Wang P, Hendrich K, Kim S-G. 2005; Spatial specificity of cerebral blood volume-weighted fMRI responses at columnar resolution. Neuroimage. 27(2):416–424. [PubMed: 15923128]

Zhao F, Wang P, Hendrich K, Ugurbil K, Kim S-G. 2006; Cortical layer-dependent BOLD and CBV responses measured by spin-echo and gradient-echo fMRI: Insights into hemodynamic regulation. Neuroimage. 30(4):1149–1160. [PubMed: 16414284]

Zhao F, Wang P, Kim S-G. 2004; Cortical depth-dependent gradient-echo and spin-echo BOLD fMRI at 9.4T. Magn Reson Med. 51(3):518–524. [PubMed: 15004793]

Zong X, Kim T, Kim S-G. 2012; Contributions of dynamic venous blood volume versus oxygenation level changes to BOLD fMRI. Neuroimage. 60(4):2238–2246. [PubMed: 22401759]

Highlights

- Reviewed layer-specific fMRI studies in animal models
- Localization of BOLD and other fMRI contrasts to true site of neuronal activity
- History of laminar studies in visual and somatosensory cortices and olfactory bulb
- Future of laminar fMRI with targeted optogenetic stimulation

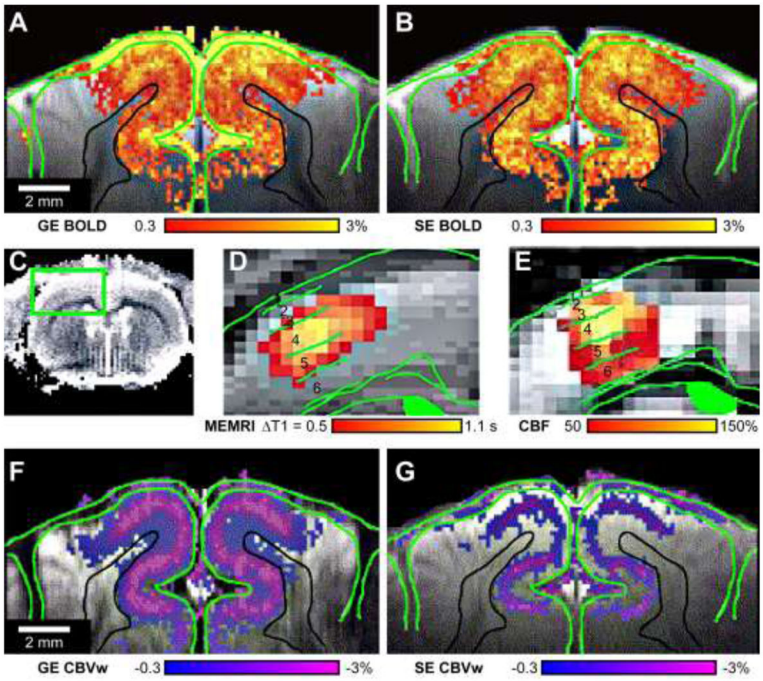

Figure 1. Suitability of different fMRI contrasts to measure layer-specific neuronal activity

Gradient-echo (GE) BOLD is the leading fMRI contrast. However, its signal changes originate from a complex interaction of cerebral blood flow (CBF), cerebral blood volume (CBV), and cerebral metabolic rate of oxygen ($CMRO_2$) increases; and is dominated by hemodynamic changes in nonspecific vascular compartments, especially veins. For stimulation of the cat visual cortex, the largest synaptic input occurred in middle cortical layers but GE BOLD activations (A) were greatest on the cortical surface (surrounded by green lines) at the location of large pial vessels, which progressively decreased toward deeper layers (black lines delineate deepest edge of the cortical gray matter). Spin-echo (SE) BOLD (B) had decreased activity at the cortical surface and increased localization to the neuronal inputs in middle layers (i.e., increased layer-specificity) compared to GE BOLD, but had reduced sensitivity. Non-BOLD fMRI contrasts that examine a single hemodynamic component have increased layer-specificity. In the primary somatosensory cortex of a single representative rat during forepaw stimulation (C), manganese-enhanced MRI (MEMRI), which is sensitive to longitudinal relaxation time (T1) changes caused by manganese ions that enter evoked neurons through voltage-gated calcium ion channels, showed the greatest neuronal activity in layer 4 (D). Similarly, CBF changes from a different rat measured by arterial spin labeling were also greatest in this layer (E). Contrast-enhanced cerebral blood volume-weighted (CBVw) fMRI with intravascular injection of monocrystalline iron oxide nanoparticles (MION) also had excellent layer-specificity in the cat visual cortex with peak activations in the middle layers, regardless of whether GE (D) or SE (E) sequences were used. This supports a microvascular origin for fMRI studies using MION, even with GE sequences. Decreases in CBVw signals indicate CBV increases. Fig. 1A, B, F, and G were adapted from Zhao et al. (2006) and C–E from Duong et al. (2000b).

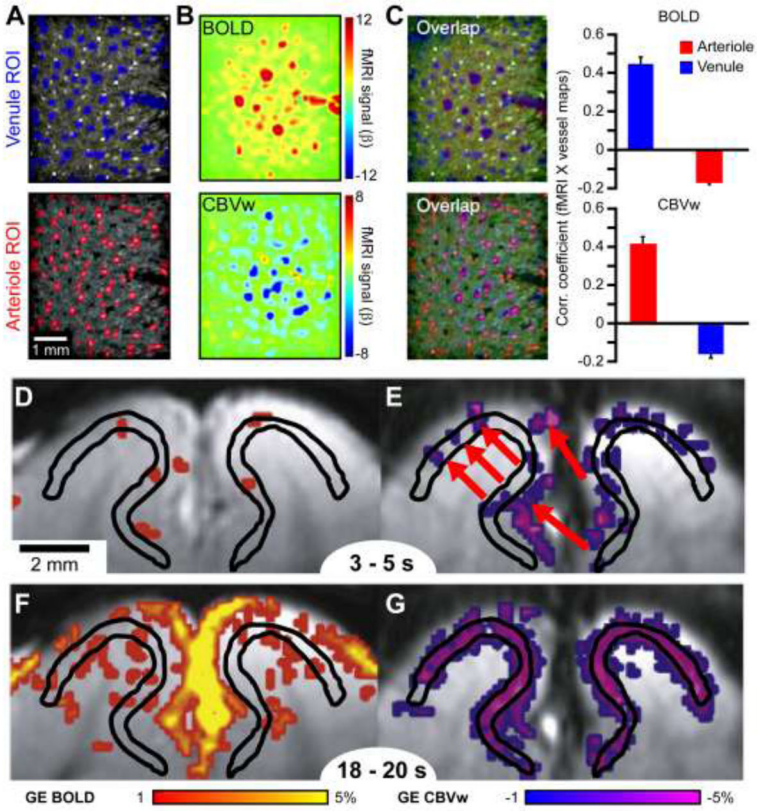

Figure 2. Vascular origins of GE BOLD and CBVw fMRI and their time dependencies

Vascular T2*-maps (A), using a multiple gradient-echo technique, and BOLD and CBVw fMRI activation maps (B) at a single, midcortical depth of the rat primary somatosensory cortex were compared at resolutions capable of discerning individual venules (blue regions-of-interest (ROI) masks, black on vascular map) and arterioles (red ROI masks, white on vascular map) to reaffirm the signal sources of these two contrasts. BOLD activations to short forepaw stimulations (<5 s) spatially corresponded to venules, while CBVw activations were localized to arterioles (C). Because both contrasts appear poorly layer-specific, contradictory to evidence presented in Fig. 1, the time dependencies of the BOLD and CBV changes are important. Specifically, shorter stimulations in the cat visual cortex were shown to be more layer-specific with BOLD fMRI (D), before venule contributions dominated, while CBVw signals were more nonspecific (E) when penetrating arteriole dilations were prominent (red arrows). On the contrary, longer stimulations evoked more nonspecific venous contributions for BOLD (F) and more specific microvascular compartments for CBVw fMRI (G). Black lines surround neural-specific middle layers and CBVw signal decreases indicate CBV increases. Fig. 2A–C were adapted from Yu et al. (2016) and D–G from Jin and Kim (2008a).

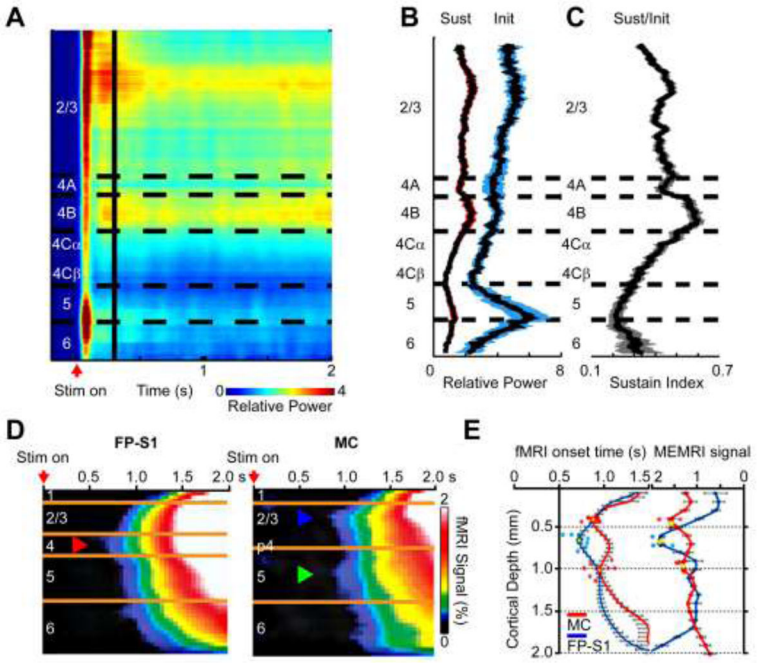

Figure 3. Dynamics for the cortical depth dependent power of gamma-band LFP and fMRI

LFPs were recorded from all the layers in the primary visual cortex of anesthetized monkeys during visual stimulation of a 2-s long drifting sinusoidal grating. The powers of the gamma-band LFP were plotted as a function of cortical depth and time (A); horizontal axis represents the time after stimulus onset, and colors represent the power of the gamma-band frequency. Horizontal dashed lines indicate the boundary of each cortical layer. The vertical line indicates 300 ms after stimulus onset. On the border of this time point, the LFPs were divided into the initial transient (Init, 0 – 200 ms) and the subsequent sustained (Sust, 300 – 2,000 ms) components. The highest power for the initial component was in layer 5/6, while the highest for the sustained component was in layers 4 and 2/3. The temporally averaged sustained (red-shaded curve) and initial transient (blue-shaded curve) components of the gamma-band LFP power were separately plotted as a function of cortical depth (B). To normalize the different input strengths to the different layers, the ratio of the sustained gamma power over the transient gamma power was plotted as a function of cortical depth (C). The normalized power of the gamma-band LFP peaked in layer 4. The shaded regions in B and C represent the standard error of the mean for all the recording sites. (D – E) High spatial (50 μm) and temporal (50 ms) resolution line scanning fMRI was used to examine the layer-specificity of the early GE BOLD response. During forepaw stimulation, the earliest response was in layer 4 (red arrowhead) of the forepaw region of the rat primary somatosensory cortex (FP-S1), where strong thalamocortical inputs are prevalent; while during whisker pad stimulation, the earliest responses were in layers 2/3 (blue arrowhead) and 5 (green arrowhead) of the motor cortex (MC), where strong corticocortical inputs from whisker S1 regions are prominent (D). The layer-specificity of these fast signal changes were consistent with the peak MEMRI responses (yellow dots), a more direct reporter of increased synaptic activity (E, MEMRI signal x1,000). Fig. 3A–C were adapted from Xing et al. (2012) and D and E from Yu et al. (2014).

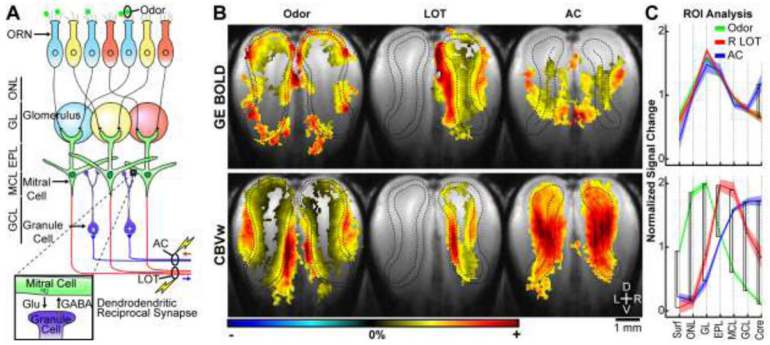

Figure 4. CBVw fMRI has excellent layer-specificity when different layers are preferentially evoked in the rat olfactory bulb

Previous layer-specific CBVw studies consistently observed the largest fMRI activations in cortical input layers where, subsequently, the largest resting microvessel blood volume pool was also located. Therefore, it was unknown whether the CBVw responses were truly neural-specific or were, instead, a mere reflection of this baseline microvascular compartment. To test this, we chose the olfactory bulb model because isolated synaptic activity can be evoked in different layers using different stimulations. Specifically, odor stimulation (64 s duration, 5% amyl acetate) evoked the greatest synaptic activity in the superficial glomerular layer (GL), while electrical stimulations (64 s durations) of the lateral olfactory tract (LOT), containing the axons of the olfactory bulb output neurons, and the anterior commissure (AC), containing extrinsic feedback axons, evoked the greatest activity in the middle external plexiform layer (EPL) and the deep granule cell layer (GCL), respectively (A). The laminar fMRI responses to odor, LOT, and AC stimulations are shown. Group activation maps (B): n = 8 rats, threshold of $p < 0.025$ for voxel- and family-wise error correction (i.e., 30 voxel cluster minimum), black dashed lines surround the layer of preferentially evoked synaptic activity determined in the T2-weighted anatomical image (i.e., the grayscale underlay). Colored scale bars: ±4% for BOLD odor, BOLD AC, CBVw AC; ±6% for BOLD LOT; ±7% for CBVw LOT; ±10% for CBVw odor. For ROI analyses (C), the mean fMRI signal change of all voxels (i.e, no threshold) in each layer was normalized by the mean activity across all seven layers in each bulb hemisphere (n = 16 left and right bulbs for odor and AC stimulations, n = 8 right (R) bulbs for LOT stimulation since no activity is expected in the left). The mean activations between stimuli were compared at each layer with one-way ANOVA and two-sample t-tests (black brackets represent significance, $p < 0.01$, uncorrected). In both analyses, GE BOLD (top row) was poorly specific and was greatest in superficial layers for all three stimulations. A relative increase in the deepest layer for AC stimulation (B, top row, blue line) provided a small indication of layer-specificity. However, the peak CBVw fMRI responses (bottom row) were consistently specific to the layer of the greatest evoked synaptic activity regardless of the baseline microvessel blood volume, which is greatest in superficial GL and smallest in deep GCL (Borowsky and Collins, 1989; Poplawsky and Kim, 2014). These results support layer-specific vascular regulation and its accurate detection with CBVw fMRI. Further, these results suggest that excitation of inhibitory neurons increases BOLD and CBVw responses. ORN, olfactory receptor neuron; Glu, glutamate; GABA, gamma-butyric acid; Surf, bulb

surface; ONL, olfactory nerve layer; MCL, mitral cell layer. Fig. 4A was adapted from Sakamoto et al. (2014) and B–C from Poplawsky et al. (2015).